Modeling the Configuration of HF Electrical Antennas for Deep Bistatic Subsurface Sounding

Marc Biancheri-Astier, Valérie Ciarletti, Alain Reineix, and Charlotte Corbel

***Abstract*—In the frame of the European Space Agency's 2016 ExoMars mission, the Electromagnetic Investigation of the SubSurface (EISS) ground-penetrating radar has been designed and developed to perform deep soundings of the Martian subsurface from the surface. The EISS is designed to take advantage of the potential for bistatic radar investigations of the Martian subsurface between the fixed station (Lander) and the mobile platform (rover) and to characterize the 3-D structure and stratigraphy of the subsurface at depths ranging from 100 m to a few kilometers out to a 1-km radius around the lander. The EISS makes use of an electric dipole antenna made of two identical 35-m resistively loaded monopoles to transmit (and also receive in a monostatic mode) the high-frequency signal. However, the EISS's most innovative capability is its potential for bistatic operation, made possible by the accommodation of a small magnetic sensor on the rover (as initially planned for the ExoMars mission) which can measure the magnetic field (all three components) of the received waves whatever the direction and orientation of the rover. The aim of this paper is to show that the two monopoles of the antenna must be deployed on the surface in nearly opposite directions but not aligned to ensure good volume coverage around the transmitter. This paper is based on Finite Difference in Time Domain (FDTD) electromagnetic simulations. The simulated data have been used to study the impact of the angle between these two monopoles on the instrument performance.**

***Index Terms*—Angle of antennas, bistatic, current sources, deep sounding, ground-penetrating radar (GPR), loaded electrical antennas, Mars, modeling, reflected wave, subsurface, wave propagation.**

DESPITE several past and present missions to Mars, very little information is available on its subsurface, the outside of its polar caps, and the region within the top half meter of the surface. One of the scientific objectives of the future European Space Agency (ESA) ExoMars mission is to characterize the water/geochemical environment as a function of depth and investigate the planet subsurface to better understand the evolution and habitability of the planet. The use of a ground-penetrating radar (GPR) will provide a nondestructive way to probe the subsurface, investigate buried structures, and look for potential deep liquid water reservoirs. This rationale led Laboratoire Atmosphère, Milieux, Observations Spatiales [LATMOS—formerly the Centre d'étude des Environnements Terrestre et Planétaires (CETP)] to design and develop the GPR called the Electromagnetic Investigation of the SubSurface (EISS).

In this paper, we describe the principle of the instrument and focus on the performance of its electric antennas. Finite Difference Time Domain (FDTD) simulations are used to model the decrease of the current along one monopole and to study the radiation pattern obtained by the two monopoles that compose the antenna. The method used to model accurately the behavior of the two unaligned monopoles is presented and validated. The results about the impact of the angle between the two monopoles are given for both the direct and reflected signals.

I. EISS: HF GPR

A. Description and Operating Principle

LATMOS designed and developed its first high-frequency (HF) GPR to perform deep soundings of the Martian subsurface from the surface in the frame of the Centre National d'Études Spatiales (CNES) Netlander mission canceled in 2004 [1], [2]. Further development work and experimental validations [4], [10]–[12] were carried out with a demonstrator called the Terrestrial and Planetary Imaging Radar (TAPIR). The EISS GPR, discussed at length here, is the updated version of the TAPIR and has been developed in the frame of the ExoMars mission.

The EISS is an impulse radar operating at HF central frequencies (∼2–4 MHz). In order to perform deep soundings of the subsurface down to kilometric depths beneath the surface, the radar needs to operate at frequencies which are as low as possible. The HF range provides a good compromise between the penetration achievable, and the size of the antenna (which is commensurate with the wavelength). The expected spatial resolution ($<$ 100 m) requires relatively short pulses (1 μs), which correspond to a bandwidth approximately equal to 1 MHz in the frequency domain.

The EISS makes use of one electric dipole antenna made of two 35-m resistively loaded monopoles ($\lambda/4$ at 2 MHz) that are deployed from the lander to transmit (and also receive in a monostatic mode) the signal. The resistive profile of each monopole must be carefully optimized to transmit the pulse without a noticeable distortion and to avoid ringing. Since the actual behavior of the antenna depends on the electromagnetic properties of the planet's regolith [10], [19]–[22], their probable range needs to be known to a reasonable accuracy.

Manuscript received February 24, 2010; revised May 21, 2010; accepted August 6, 2010.

M. Biancheri-Astier, V. Ciarletti, and C. Corbel are with the Laboratoire ATmosphère, Milieux, Observations Spatiales (LATMOS), Université Versailles Saint-Quentin, Centre National de la Recherche Scientifique/Institut National des Sciences de l'Univers, LATMOS-Institut Pierre Simon Laplace, 78280 Guyancourt, France (e-mail: marc.biancheriastier@latmos.ipsl.fr).

A. Reineix is with the XLIM Institut de Recherche, 87060 Limoges CEDEX, France.

Digital Object Identifier 10.1109/TGRS.2010.2070513

In order to explore a subsurface area as large as possible, it is essential to work with nondirective antennas which have a large radiating pattern within the subsurface. More specifically, since the EISS is designed to take advantage of the potential for bistatic radar investigations of the subsurface between the ExoMars lander and the small magnetic antenna and receiving unit on the rover, the two monopoles must be deployed on the surface at an angle which ensures good volume coverage all around the transmitter. The receiving antenna can be oriented along three perpendicular directions to ensure the reception of the signal whatever the direction and orientation of the rover.

Operating a GPR from the surface significantly limits the areal extent of the potential study area but eliminates the ionospheric interference and attenuation experienced by orbital radar sounders like Mars Advanced Radar for Subsurface and Ionosphere Sounding (MARSIS) [9], [13]–[15] and Shallow Radar (SHARAD) [3], [16]. Moreover, a sounder on a stationary lander can perform coherent additions of the reflected signal, significantly improving the signal-to-noise ratio and, thus, the detection of very weak signals. Based on this approach, the EISS can be used to characterize the structure and stratigraphy of the subsurface at depths ranging from 100 m to a few kilometers out to a 1-km radius around the lander.

The EISS is mainly a GPR, but the presence of electrical monopoles deployed on the surface enables consideration of other operating modes without additional equipment. The EISS can operate in four modes:

- *monostatic sounding of subsurface* (emission and reception of HF radar waves, utilizing two fixed electrical monopole antennas) for the characterization of deep geological structures below a fixed station;
- *bistatic sounding of subsurface* (radar emission with two fixed monopole HF electrical antennas and reception with a small rover-mounted magnetic antenna) for the 3-D location and characterization of deep geological structures between stations;
- *HF electrical monopole impedance measurement* for the estimation of the geoelectrical characteristics of the near-surface Martian regolith;
- *passive modes* for the monitoring of the HF background noise at the Martian surface, which may originate from the atmospheric electrical activity and variations in the electron density and plasma frequency of the ionosphere.

The results presented in this paper focus on the bistatic sounding mode. Electromagnetic simulations have been used to optimize the value of the angle between the two monopoles, its impact on the radiation pattern of antennas, and the volume coverage around the fixed station.

B. Schematic Description of Instrument

The EISS is mainly composed of two units (see Fig. 1):

1) on the lander platform (GPR1):
   - two HF electrical monopoles which constitute the transmitting (and receiving) antennas and which are used for all operating modes of the instrument;
   - one HF transmitter for the monostatic and bistatic surveys and impedance measurements;
   - one HF receiver for the monostatic sounding, impedance measurement, and passive modes;
   - one VHF antenna and its associated VHF transmitter for the implementation of the bistatic mode (synchronization of both the lander and rover EISS units).
2) on the rover platform (GPR2) used only for the bistatic mode:
   - one small HF magnetic sensor;
   - one HF receiver;
   - one VHF antenna and its VHF receiver.

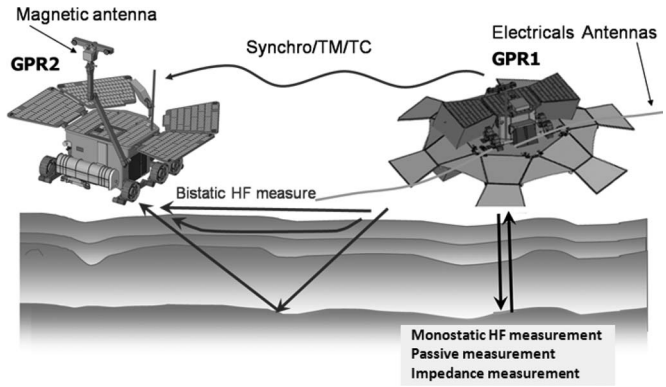

Fig. 1. EISS as it was configured for the original 2011 ExoMars mission, illustrating the different kinds of waves the receiver could have potentially detected. GPR1 is on the fixed station (lander) which both transmits and receives using its pair of electrical monopole antennas and GPR2 is on the rover, receiving with the magnetic antenna.

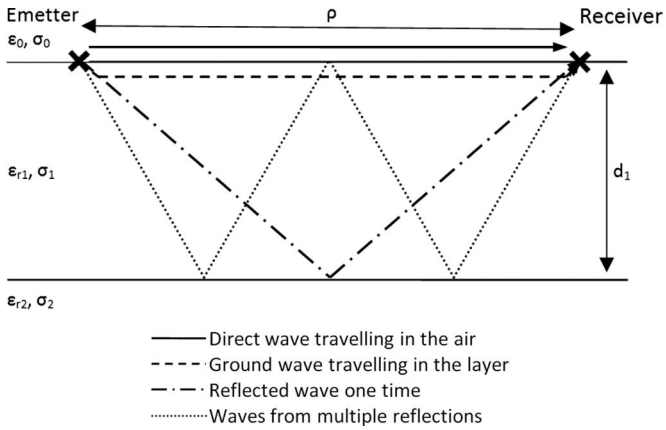

Fig. 2. Waves that can be detected in bistatic configuration.

C. Identification of Received Echoes

For simplicity, we consider a subsurface composed of one homogeneous layer d_1 m thick with a relative permittivity ε_{r1}, which overlies a homogeneous semi-infinite half-space. Fig. 2 shows the different kinds of waves potentially received in the bistatic mode.

The propagation delay for the main waves can be easily calculated for a given distance ρ between the transmitter and

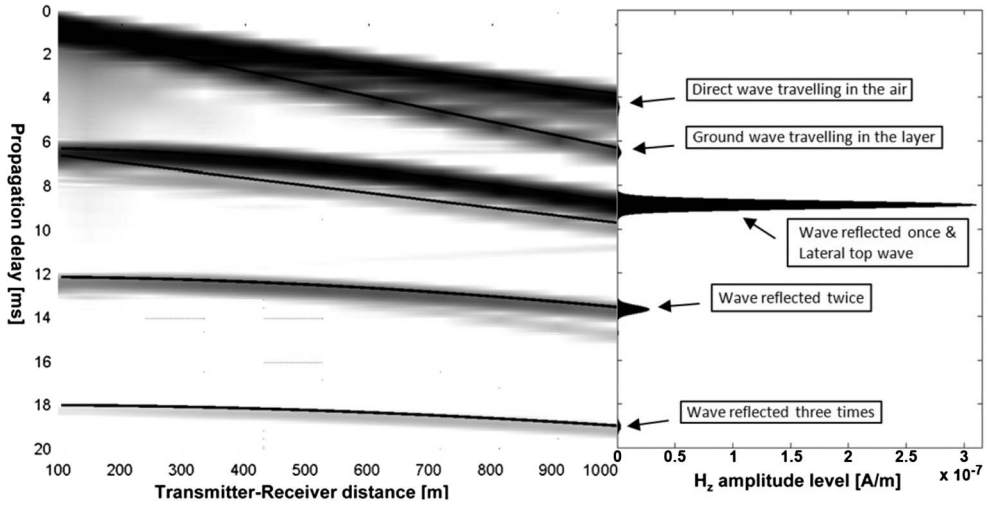

Fig. 3. Example of radargram showing the envelope of the received signal (H_z) as a function of the distance between the transmitter and the receiver. Top layer is 500 m thick and has a relative permittivity of $\varepsilon_{r1} = 4$ and $\sigma = 0$. Direction between the transmitter and receiver makes an angle of 45° with respect to the direction of the transmitting electrical antenna.

the receiver (the vacuum wave speed and the celerity c):

- direct wave traveling in the air

$$t_{\mathrm{AIR}}(\rho) = \frac{\rho}{c} \tag{1}$$

- ground wave traveling in the layer

$$t_{\mathrm{SOIL}}(\rho) = \frac{\rho\sqrt{\varepsilon_{r1}}}{c} \tag{2}$$

- waves reflected n times in the first layer

$$t_{\mathrm{REFLECTED\_}n}(\rho) = \frac{\sqrt{\rho^2 + (n \cdot 2 \cdot d_1)^2} \cdot \sqrt{\varepsilon_{r1}}}{c}. \tag{3}$$

The radargram (see Fig. 3) shows the echoes received according to their time of arrival when the distance between stations ρ varies from 100 to 1000 m. In the example of Fig. 3, the amplitude of the reflected signals is particularly high because of the null conductivity of the simulated environment and of the perfectly reflecting horizontal layer placed at the bottom of the 500-m-thick layer. More realistic environments will result in reflected signals much weaker than the direct ones.

II. Modeling of Unaligned Monopoles

In the context of the ExoMars mission, the exact value of the angle between the two electric monopole antennas will likely be imposed by the platform design and will be chosen to minimize the contact between the antennas, the platform and solar panels, keeping the radiation pattern as omnidirectional as possible. This is essential given the fact that the location of the rover and its onboard receiver cannot be anticipated. In the following discussion, we present our analysis of how the angle between the monopoles impacts the radiation pattern and performance characteristics of the EISS GPR.

A. Modeling Approach

In order to study the impact of the antenna configuration (i.e., the angle between the two monopoles) on the instrument performance, numerical simulations have been run. A numerical code operating in the time domain is perfectly suited to describe the pulse interaction and propagation through the subsurface. Previous studies [4], [10] have shown that the coupling between the monopoles and the surface cannot be neglected and depends on the geoelectrical properties of the regolith [6], [8].

The Time Electromagnetic Simulator Finite Difference (TEMSI-FD) Simulator code chosen is an FDTD numerical code developed at Limoges (XLIM) that allows an accurate modeling of the end-to-end operation of the radar. It is able to accurately model the dual resistively loaded monopole antenna system as well as the potentially complex structure of the subsurface. The computational volume is divided in rectangular cells, each of which is characterized by its permittivity and conductivity values [5], [7], [18]. Absorbing walls or conformal perfectly matched layers are used in order to avoid parasitic reflections at the borders of the finite computational volume.

The available version of the TEMSI-FD we used is able to take into account the exact design of the monopoles with their wires and resistors as long as they are located on the orthogonal mesh of the computational volume, which makes this code inappropriate for the case of unaligned monopoles.

It was thus necessary to find an equivalent representation of a monopole that is suitable for both aligned and unaligned monopoles. The method we used is based on the fact that the physical resistively loaded monopole behaves like a series of theoretical current sources distributed along the monopole length. The distance between two consecutive sources is chosen to ensure that all the sources are located at an intersection point of the mesh. Each of theses fictive sources generates a current that has the HF excitation pulse shape with an amplitude and a delay that depend on its own location along the antenna. For the chosen distance between sources, the set of amplitudes and delays is obtained by a simulation performed for a

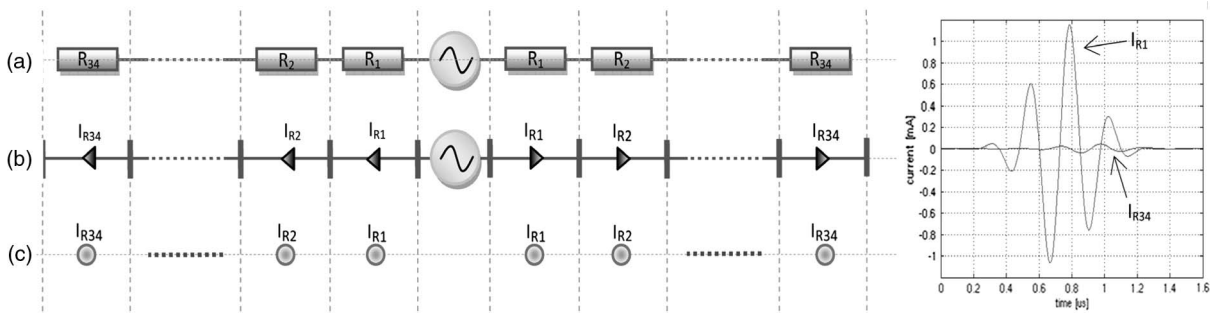

Fig. 4. Modeling approach with the orthogonal mesh. (a) Physical representation of one monopole with wires and resistors. (b) Representation of the current along the antenna. (c) Representation of the same monopole with current sources. Plots on the right show the time function describing the shape of the excitation at the beginning (I_{R1}) and at the end (I_{R34}) of the monopole for a subsurface permittivity equal to four.

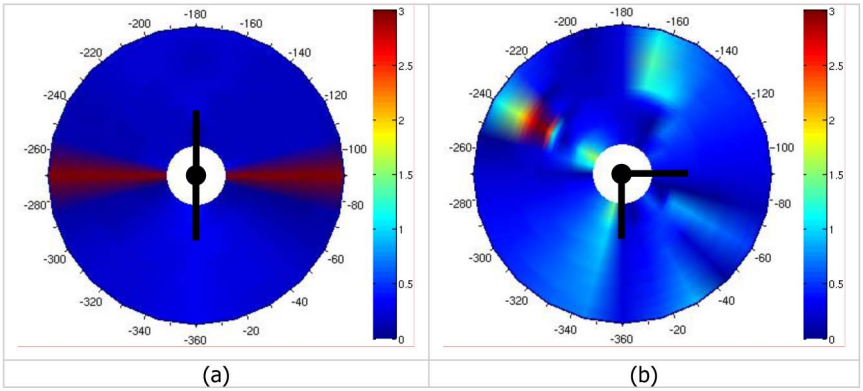

Fig. 5. Maps of the difference [in logarithmic scale (decibels)] between the results obtained with the model based on point current sources versus the ones obtained with the exact design of the monopoles with their wires and resistors. Maps show, as an example, the amplitude of the H_y magnetic component for the direct wave computed for two different configurations of antennas. (a) Two aligned monopoles $\theta_{\text{antennas}} = 180°$. (b) Two perpendicular monopoles $\theta_{\text{antennas}} = 90°$.

monopole aligned on the mesh (see Fig. 4). It is essential that the geoelectric properties assumed in the simulation are similar to those of the actual subsurface environment [10], [19]–[22]. This approach has been validated for simple cases that could be modeled by either a series of point current sources or directly with the wire and resistors of the loaded monopole.

In the case of two aligned monopoles, the error in the amplitude computed with the current sources versus the amplitude computed with the wire and resistors is less than 0.4 dB for more than 80% of the receiver locations. This is equivalent to the error in the amplitude of the received signal that would result from a 5% error in the distance between the transmitter and receiver. With the antenna made of two perpendicular monopoles, 47% of the receiver locations show an error less than 0.4 dB, and 91% have an error less than 0.8 dB. The strongest discrepancies happen where the signal is very weak and where the accuracy of the results can be questioned. As a consequence, we can consider that the modeling based on the current sources is validated and will be used in the following paragraphs. Fig. 5 illustrates the results obtained for the H_y magnetic component.

B. Amplitude of the Current Sources

The HF pulse used to probe the subsurface is a wideband signal, and a simple wire antenna cannot guarantee, over the radar's full bandwidth, that a null current will exist at the end of each monopole, which is necessary to avoid the ringing due to the reflections at the end of the antenna. To protect against this possibility, the resistive distribution along the antenna is calculated to obtain a purely progressive wave, thereby eliminating any ringing. Wu *et al.* have proposed, for an antenna surrounded by vacuum, a method to calculate a resistive distribution along the antenna [17].

The EISS electrical antenna is designed to be deployed on the surface of the planet, and since a significant coupling with the regolith will occur, the actual performance of the antenna will depend on both the regolith geoelectrical properties and the resistive profile chosen for the antenna. The resistive profile will be optimized according to an *a priori* estimated value of the regolith permittivity $\varepsilon_{r-\text{opt}}$ while the antenna will be deployed on a surface which is likely to have a different permittivity value $(\varepsilon_{r-\text{soil}})$.

A future paper will be dedicated to the optimization of the resistive profile. For the purpose of this paper, the resistive profile used for all the simulations is the one that is optimized for a relative permittivity equal to four. This value seems to be a reasonable value for the Martian regolith [6], [8] and is the one that was chosen for the ExoMars mission. Fig. 6 shows the decrease of the current obtained by numerical simulation with the TEMSI-FD along a monopole when deployed on a layer characterized by its relative permittivity $\varepsilon_{r-\text{soil}}$ and

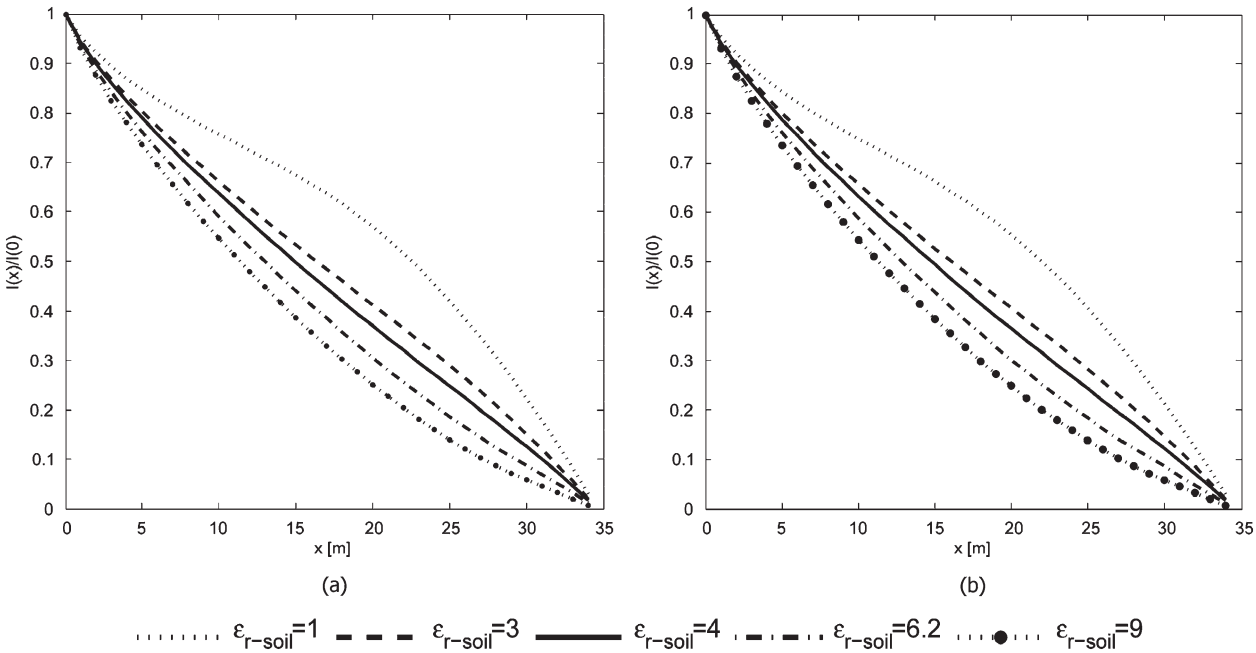

Fig. 6. Current distribution along the loaded monopole which is optimized for a permittivity of the first layer equal to four, as a function of the relative permittivity of the subsurface $\varepsilon_{r-\mathrm{soil}}$. Conductivity of the subsurface equal to (a) $\sigma = 0$ or (b) $\sigma = 10^{-5}$ S $\cdot$ m^{-1}.

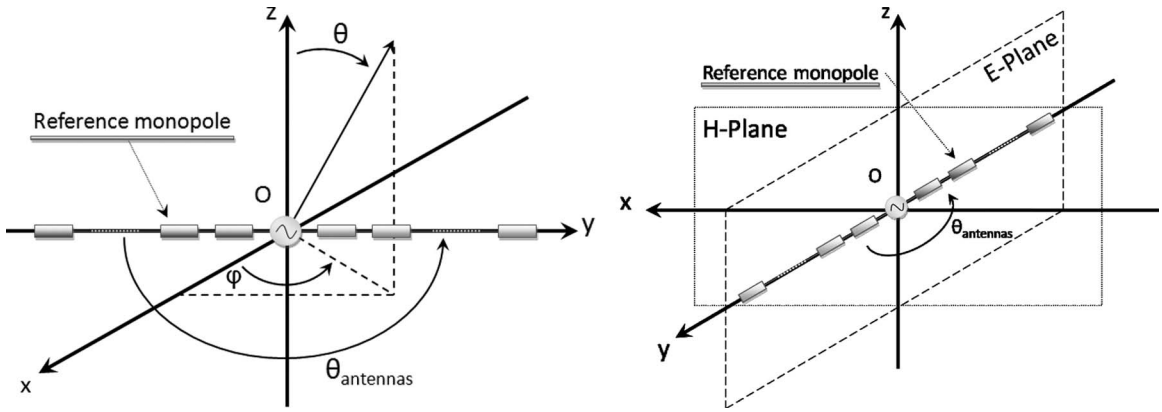

Fig. 7. Definition of the φ, θ, and $\theta_{antennas}$ angles and E and H planes.

its conductivity σ. These current values obtained along the monopole will be used as inputs for the amplitude of the current sources in the following simulations.

III. Impact of the Angle Between the Two Monopoles of the HF Antenna

The two monopoles need to be deployed on the surface in a way that ensures coverage that is as omnidirectional as possible around the transmitter. Electromagnetic simulations have been run to study the impact of different potential configurations. Three different configurations of the antennas are shown and compared in the following: 1) one single transmitting monopole aligned along the O_y-axis that illustrates the minimal configuration; 2) two transmitting monopoles perfectly aligned along the O_y-axis which is considered as the reference configuration (called the dipole in the following); and 3) two unaligned transmitting monopoles. For the unaligned configuration, the results are given in this paper for the reference monopole aligned along the O_y-axis, and the second monopole deployed at an angle $\theta_{\mathrm{antennas}}$ equal to 225° with respect to the O_y-axis. The 225° angle value is the one that was imposed for the ExoMars mission by the solar panel configuration.

A. Radiation Pattern

The radiation pattern is obtained in a far field for the case where the antenna is deployed on a homogeneous subsurface (a permittivity equal to four as an example). The geometry and the angles for the studied configurations are described in Fig. 7. The E plane corresponds to $\varphi = 0°$ and $0° < \theta < 360°$ while the H plane is perpendicular to the antenna ($\varphi = 90°$ and $0° < \theta < 360°$).

In order to be able to compare the results obtained for the three different antenna configurations, for different permittivity

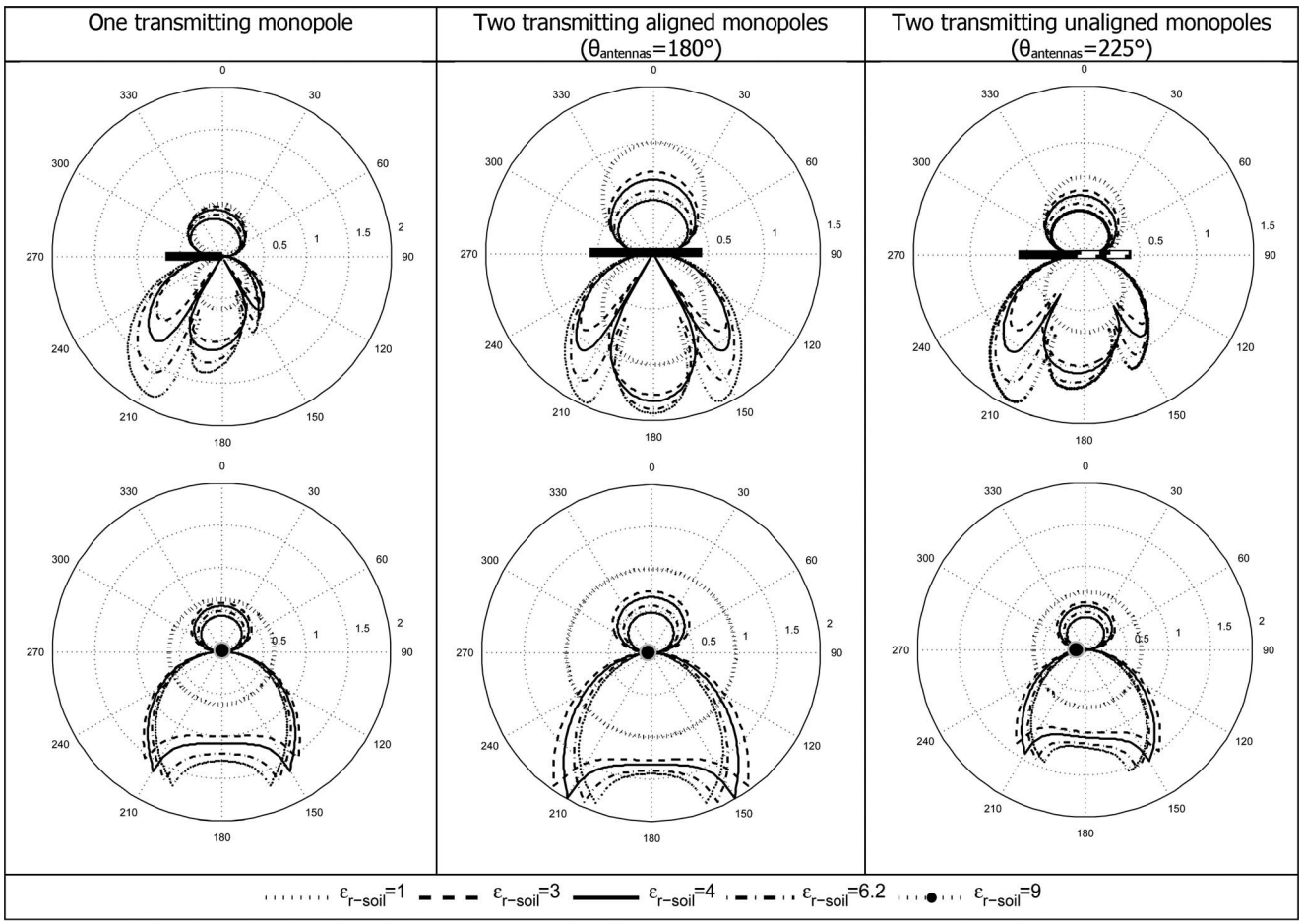

Fig. 8. Radiating patterns in the E and H planes for different configurations of antennas, deployed on a homogeneous subsurface ($\sigma = 0$ and $f = 2$ MHz). Diagram obtained for antenna(s) deployed in vacuum is the reference (normalized). All patterns are normalized by the radiating pattern of two transmitting aligned monopoles in vacuum. (The profile antenna is optimized for a relative permittivity of the first layer equal to four.)

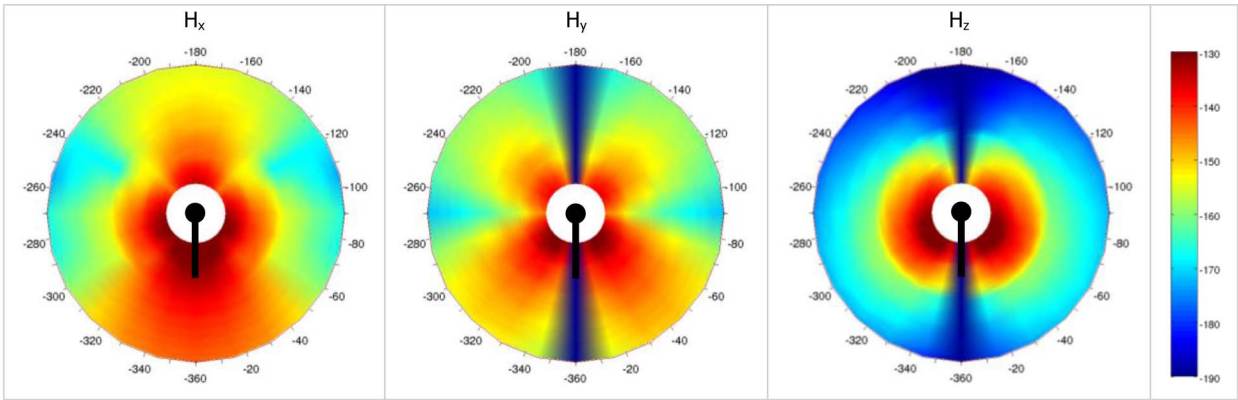

Fig. 9. Amplitude [in logarithmic scale (dBA/m)] of the magnetic field corresponding to the direct wave for a transmitter–receiver distance ranging from 100 to 500 m. (Black) Transmitting antenna is a single monopole.

values of the subsurface regolith, all patterns shown in the following are normalized by the maximum value obtained with an aligned dipole in vacuum.

Fig. 8 shows that the amplitude of the transmitted signal into the subsurface increases when the relative permittivity of the subsurface increases, whatever the configuration of the antennas is. Each radiation pattern in the subsurface clearly shows very weak values for some specific directions, which can potentially lead to coverage problems. Nevertheless, the representations of the radiation pattern fail to provide a clear understanding of the coverage obtained in the area around the transmitter and, most of all, only consider the wave propagating directly from the transmitter to the receiver. Given the fact that the information about the subsurface structure is provided by the reflected waves, a more adapted representation will be used in the following sections.

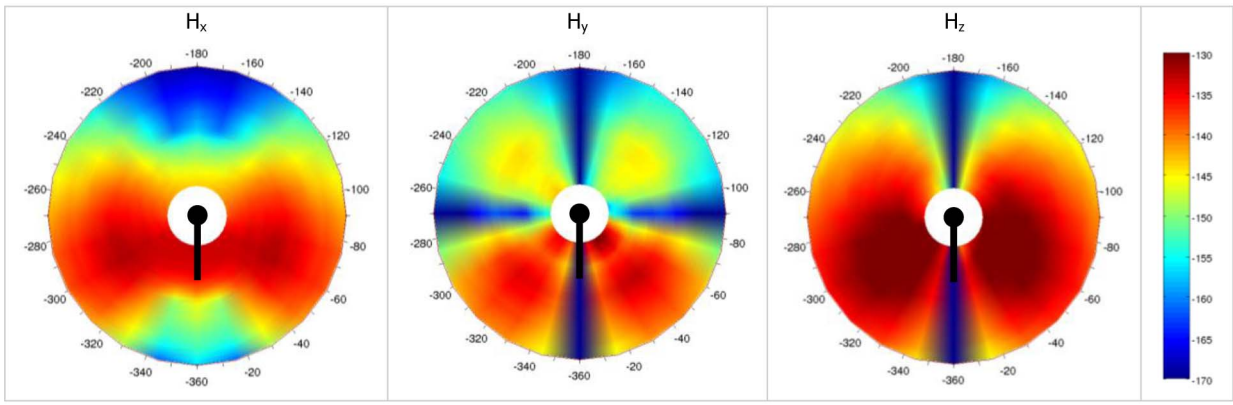

Fig. 10. Amplitude [in logarithmic scale (dBA/m)] of the magnetic field corresponding to the reflected wave for a transmitter–receiver distance ranging from 100 to 500 m. (Black) Transmitting antenna is a single monopole.

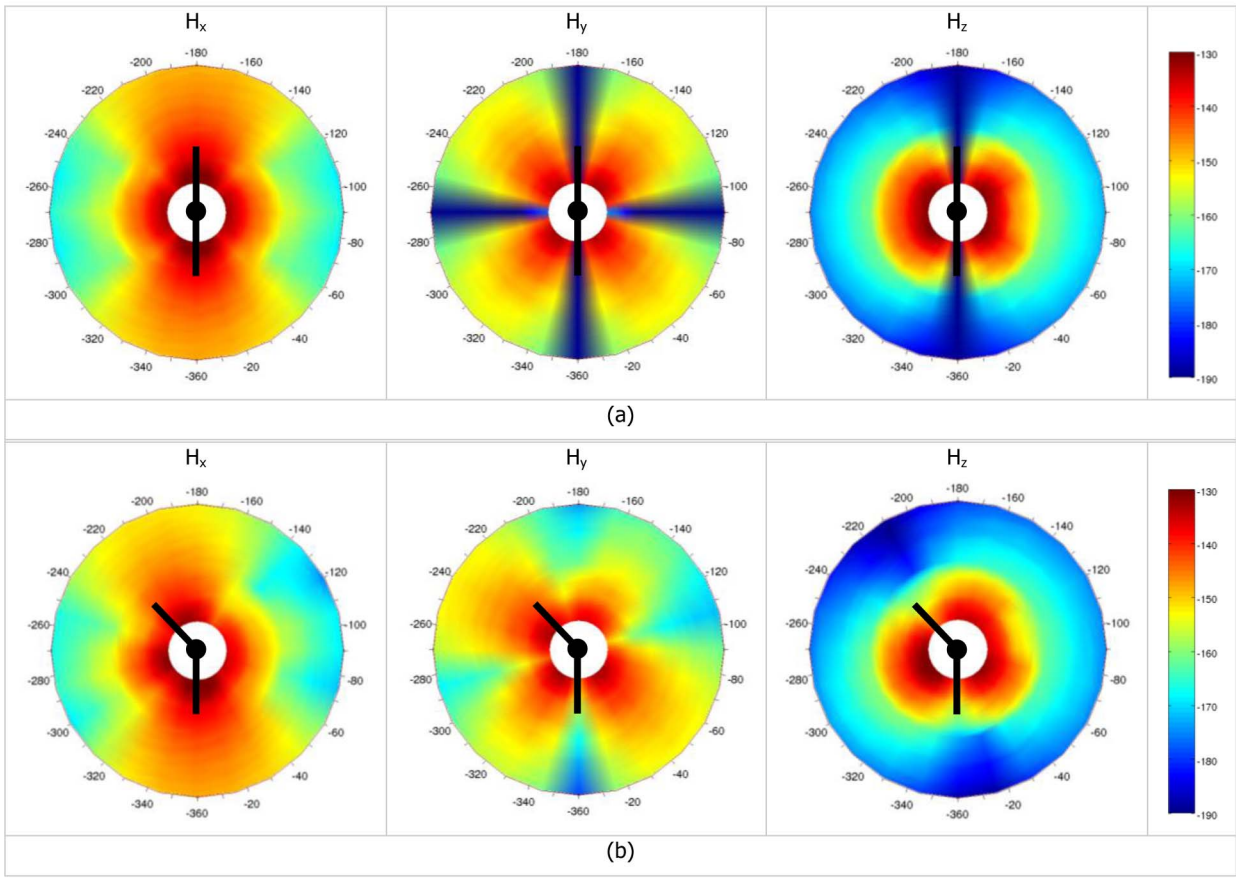

Fig. 11. Amplitude [in logarithmic scale (dBA/m)] of the magnetic field corresponding to the direct wave for a transmitter–receiver distance ranging from 100 to 500 m. (Black) Transmitting antenna is made of (a) two aligned monopoles and (b) two unaligned monopoles $\theta_{\text{antennas}} = 225°$.

B. Magnetic Field Obtained at the Receiver for Various Configurations

In the bistatic operating mode, the receiving sensor is a magnetic antenna (small enough to be accommodated on a mobile platform) that can be oriented along three perpendicular directions to measure the three components of the magnetic field at the rover's location. Numerical simulations have been run to obtain maps of the magnetic field generated by the different configurations of the transmitting electric antenna. Both the direct and reflected waves have been considered separately.

The subsurface considered for the simulation is composed of a 100-m-thick homogeneous layer (with a permittivity value of $\varepsilon_{r1} = 4$ and a conductivity value of $\sigma = 10^{-5}$ S $\cdot$ m^{-1}) on the top of a second layer of infinite thickness (with a permittivity value of $\varepsilon_{r2} = 9$ and the same conductivity value of $\sigma = 10^{-5}$ S $\cdot$ m^{-1}). This subsurface structure is a particularly simple one but will allow the study of the reflection that occurs at the interface between the two layers. For each antenna configuration and each detected wave (either direct or reflected), the amplitudes of the three components of the magnetic field

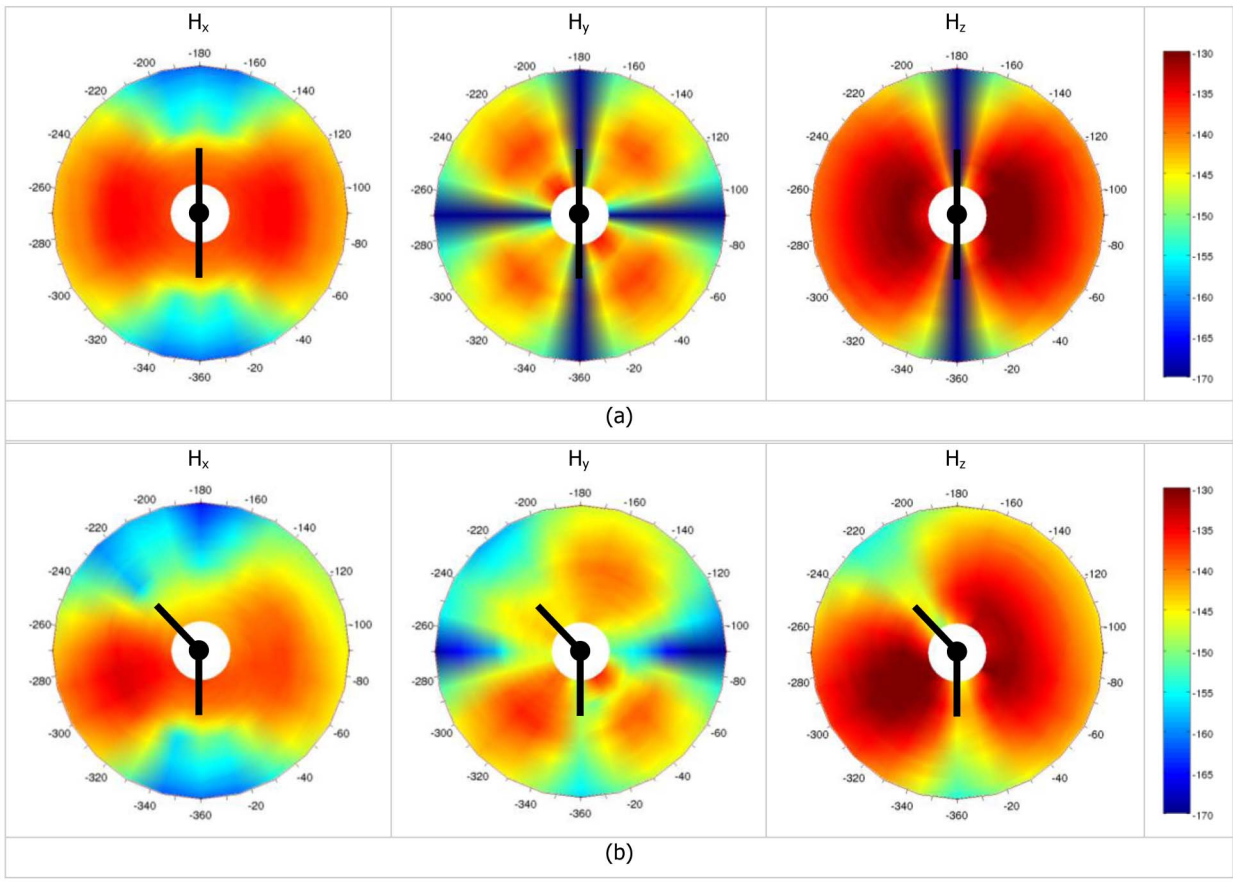

Fig. 12. Amplitude [in logarithmic scale (dBA/m)] of the magnetic field corresponding to the reflected wave for a transmitter–receiver distance ranging from 100 to 500 m. (Black) Transmitting antenna is made of (a) two aligned monopoles and (b) two unaligned monopoles $\theta_{\text{antennas}} = 225°$.

are computed. The values obtained when the receiver is located anywhere within 100–500 m of the transmitter are presented in a series of maps. The values are given in a logarithmic scale (see Figs. 9–12).

1) Magnetic Field Obtained With One Transmitting Monopole:

Direct wave amplitude: The direct amplitude maps are displayed in Fig. 9. They clearly show that, as expected, the amplitude of the wave that travels directly from the transmitter to the receiver is much weaker if the receiver is not located in the monopole direction. The direct wave does not give any information about the subsurface but will provide a reference for both the propagation delay and amplitude. The measured delay should be consistent with the distance between the transmitter and the receiver, and the amplitude will provide a way to get calibrated data.

Reflected wave amplitude: Fig. 10 corresponds to the amplitude of the wave reflected by the interface buried at 100 m below the surface level, which is the one we are mainly interested in. The maps clearly show that a large percentage of the receiver locations would receive a very weak signal whatever the orientation of the receiver is. The use of a single monopole would make sense only if the receiver location could be chosen to avoid these problematical areas. The simulations have been performed for a horizontal interface; in case of an inclined one, the behavior would be very similar, but the exact location of nonfavorable locations would not be exactly the same.

2) Magnetic Field Obtained With Two Transmitting Monopoles: The previous section has shown that the use of one single monopole to transmit the signal is not suitable; simulations have thus been made to compute the coverage obtained by the two monopoles deployed in roughly opposite directions. The same magnetic field maps have been generated for the two other configurations previously described: a) two transmitting aligned monopoles also noted as the dipole ($\theta_{\text{antennas}} = 180°$) and b) two transmitting unaligned monopoles ($\theta_{\text{antennas}} = 225°$).

Direct wave amplitude: Fig. 11 presents the results for the direct wave. Fig. 11(a) with the aligned monopoles clearly brings to light the fact that, in some directions (aligned with and perpendicular to the antenna direction), one or two of the components are almost zero while the unaligned monopoles [see Fig. 11(b)] do not create such problematic features. The configuration with the unaligned monopoles does offer the best coverage of the whole area.

The comparison of the maps in Fig. 11 shows that 50% of the locations see a stronger signal when the monopoles are not aligned than with the aligned dipole configuration. The increase of the received amplitude can reach 80 dB, in the directions parallel and perpendicular to the reference monopole, for the H_y and H_z components. In return, weaker damage between 0 and 10 dB is to be deployed for some locations where the signal amplitude was particularly large with a dipole. The radiation of the magnetic field (and electrical fields too)

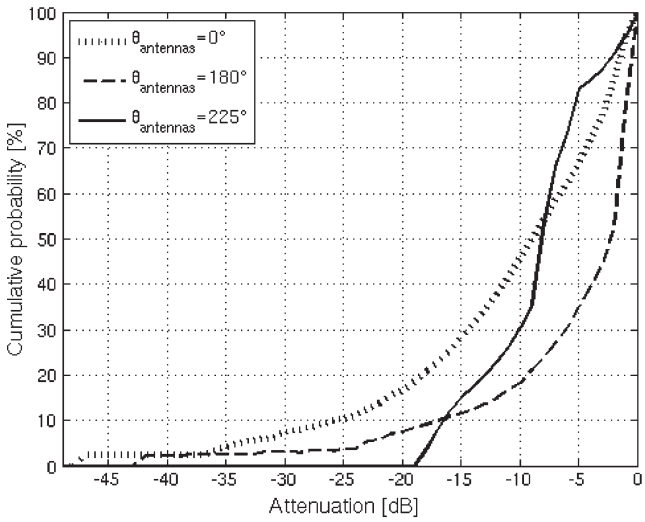

Fig. 13. Cumulative probability to encounter an attenuation compared to the best situation larger than the abscissa. Abscissa values correspond to the magnetic field module of the reflected wave. Distance between transmitter and receiver is 500 m. Subsurface characteristics are as follows: $\varepsilon_{r1} = 4$, $\sigma_1 = 10^{-5}$ S $\cdot$ m^{-1}, and $d_1 = 100$ m; $\varepsilon_{r2} = 9$ and $\sigma_2 = 10^{-5}$ S $\cdot$ m^{-1}.

will be more omnidirectional by using the unaligned monopoles configuration.

Reflected wave amplitude: Fig. 12 shows the results for the reflected wave due to an interface buried at 100 m below the surface. The configuration with the unaligned monopoles optimizes the coverage of the whole area and minimizes the problematic areas.

The comparison of the maps in Fig. 11 leads to the same conclusion as for the direct wave: The radiation of the magnetic field (and electrical fields too) will be more omnidirectional if the unaligned monopole configuration is used.

3) Study Summary of Magnetic Field Obtained With Different Configurations: Fig. 13 summarizes the situation. It shows, for each of the studied configurations, the probability of encountering an attenuation larger than the abscissa value. The reference for this attenuation is the maximum value obtained for the module of the magnetic field at 500 m from the transmitter.

For example, in case of the unaligned monopoles ($\theta_{\text{antennas}} = 225°$), the probability of encountering an attenuation stronger than 19 dB, compared to the most favorable direction, is null while it goes up to approximately 8.5% for the aligned dipole configuration and to 19% for the configuration with one monopole only. The configuration with the two unaligned transmitting monopoles ensures the most homogeneous area coverage around the fixed station.

IV. Discussion and Conclusion

The aim of this paper was to study the transmitting antenna configuration that would allow the best use of a bistatic GPR (involving a lander and a rover operating from the planet's surface). The results presented are based on numerical FDTD simulations that allowed the modeling of the electromagnetic field generated by the electric antennas while taking into account the coupling between each monopole and the subsurface. A new numerical modeling approach for unaligned electrical monopoles has been presented and used to get reliable results. Radiation patterns and cartographies of the magnetic field for both direct and reflected waves in the vicinity of the transmitting antennas have been obtained. This paper has demonstrated that the angle between the two monopoles has a significant impact on the instrument performance. We have concluded that the volume coverage capability of the GPR is clearly enhanced if unaligned monopoles are used for transmission. As a conclusion, the use of unaligned monopoles is mandatory.

In this paper, the subsurface was simply modeled by a single interface between two homogeneous layers; future work will take into account a more realistic subsurface model with fine scale layering and local volumetric heterogeneities. The possible effect of magnetic materials in the soil will also be considered. This can be of prime importance in accurately assessing the likely performance of a radar instrument on Mars.

Additional and complementary work is currently being done to optimize the antenna resistivity profile and to use its measured impedance to get an estimation of the geoelectrical parameters (permittivity and conductivity) of the near subsurface.

The EISS was initially part of the payload for the original ESA 2016 ExoMars mission and was designed to take advantage of the potential for bistatic radar sounding between the stationary platform/lander and mobile platform. After the last redesign of the mission, the whole lander payload was removed. However, the EISS can also perform useful measurements when operated in a monostatic mode from the individual stations of a multistation Mars network mission. Even for monostatic use, it is essential to choose an antenna configuration that ensures the coverage of a volume beneath the transmitter is as large as possible. Potential applications on Earth are, for example, the search for deep liquid water reservoirs in arid environments or the mapping of the bedrock buried under thick layers of ice.

References

[1] J. J. Berthelier, R. Ney, V. Ciarletti, B. Martinat, M. Hamelin, F. Costard, P. Paillou, C. Nevejans, W. Kofman, J. G. Trotignon, G. Grandjean, M. Zamora, and A. Nagy, "GPR, a ground-penetrating radar for the NetLander mission," *J. Geophys. Res.*, vol. 108, no. E4, p. 8027, Feb. 2003. DOI: 10.1029/2002JE001866.

[2] J. J. Berthelier, R. Ney, F. Costard, A. Meyer, B. Martinat, A. Reineix, T. Hansen, M. Bano, W. Kofman, F. Lefeuvre, and P. Paillou, "The GPR experiment on NetLander," *Planet. Space Sci.*, vol. 48, no. 12–14, pp. 1161–1180, Oct. 2000.

[3] D. Biccari, G. Picardi, and R. Seu, "Mars high resolution SHAllow RADar (SHARAD) for the MRO 2005 missions," in *Proc. Geosci. Remote Sens. Symp.*, 2002, vol. 4, pp. 2159–2161.

[4] V. Ciarletti, A. Le Gall, J. J. Berthelier, C. Corbel, F. Dolon, and R. Ney, "Bistatic deep soundings with the HF GPR TAPIR in the Egyptian white desert," in *Proc. Lunar Planet. Sci. XXXVII Conf.*, 2006.

[5] V. Ciarletti, B. Martinat, A. Reineix, J. J. Berthelier, and R. Ney, "Numerical simulation of the operation of the GPR experiment on NetLander," *J. Geophys. Res.*, vol. 108, no. E4, p. 8028, 2003. DOI: 10.1029/2002JE001867.

[6] S. M. Clifford, "A model for hydrologic and climatic behaviour of water on Mars," *J. Geophys. Res.*, vol. 98, no. E6, pp. 10 973–11 016, Jun. 1993.

[7] C. Guiffaut, Guide de l'utilisateur de TEMSI—Version 3.0, 2007.

[8] E. Heggy, P. Paillou, F. Costard, N. Mangold, G. Ruffie, F. Demontoux, G. Grandjean, and J. M. Malézieux, "Local geoelectrical models of the Martian subsurface for shallow groundwater detection using sounding radars," *J. Geophys. Res.*, vol. 108, no. E4, p. 8030, Mar. 2003. DOI: 10.1029/2002JE001871.

[9] A. Ivanov, A. Safaeinili, J. J. Plaut, S. Milkovich, and G. Picardi, "Observations of the layering structure in the Martian polar layered deposits with the MARSIS instrument," in *Proc. AGU Fall Meeting Abstract P13D-07*, San Fransisco, CA, 2006.
[10] A. Le Gall, A. Reineix, V. Ciarletti, J. J. Berthelier, R. Ney, F. Dolon, and C. Corbel, "An estimation of the electrical characteristics of planetary shallow subsurfaces with TAPIR antennas," *J. Geophys. Res.*, vol. 111, p. E06 S06, Jun. 2006. DOI: 10.1029/2005JE002595.
[11] A. Le Gall, V. Ciarletti, J. J. Berthelier, A. Reineix, C. Guiffaut, R. Ney, and F. Dolon, "An imaging HF GPR using stationary antennas: Experimental validation over the antarctic ice sheet," *IEEE Trans. Geosci. Remote Sens.*, vol. 46, no. 12, pp. 3975–3986, Dec. 2008.
[12] A. Le Gall, "Sondage des sous-sols planétaires par radar à pénétration de sol: Etude et modélisation des performances de l'instrument TAPIR," Ph.D. dissertation, CEPT Centre d'études de l'environnement terrestre et planétaire, Paris, France, 2007.
[13] G. Picardi, "Radar soundings of the subsurface of Mars," *Science*, vol. 310, no. 5756, pp. 1925–1928, Dec. 2005.
[14] J. J. Plaut, G. Picardi, A. B. Ivanov, S. M. Milkovich, A. Cicchetti, W. Kofman, J. Mouginot, W. M. Farrell, R. J. Phillips, S. M. Clifford, A. Frigeri, R. Orosei, C. Frederico, I. P. Williams, D. A. Gurnett, E. Nielsen, T. Hagfors, E. Heggy, E. R. Stofan, D. Plettemeier, T. R. Watters, C. J. Leuschen, and P. Edenhofers, "Subsurface radar sounding of the south polar layered deposits of Mars," *Science*, vol. 316, no. 5821, pp. 92–95, Apr. 2007.
[15] J. J. Plaut, "MARSIS subsurface sounding observations of the polar deposits of Mars," in *Proc. AGU Fall Meeting Abstract P13D-06*, San Fransisco, CA, 2006.
[16] R. Seu, D. Biccari, R. Orosei, L. V. Lorenzoni, R. J. Phillips, L. Marinangeli, G. Picardi, A. Masdea, and E. Zampolini, "SHARAD: The MRO 2005 shallow radar," *Planet. Space Sci.*, vol. 52, no. 1–3, pp. 157–166, Jan.–Mar. 2004.
[17] L. C. Shen and R. W. P. King, "Correction to the cylindrical antenna with non reflecting resistive loading by Wu and King," *IEEE Trans. Antennas Propag.*, vol. AP-13, no. 6, p. 998, Nov. 1965.
[18] D. Uduwawala and M. Norgren, "An investigation of some geometrical shapes and selection of shielding and lumped resistors of planar dipole antennas for GPR applications using FDTD," *IEEE Trans. Geosci. Remote Sens.*, vol. 44, no. 12, pp. 3555–3562, Dec. 2006.
[19] J. R. Wait, "Theory of wave propagation along a thin wire parallel to an interface," *Radio Sci.*, vol. 7, no. 6, pp. 675–679, Jun. 1972.
[20] D. L. Wright and J. F. Prewitt, "A radiating dipole antenna with tapered impedance loading," *IEEE Trans. Antennas Propag.*, vol. AP-23, no. 11, pp. 811–814, Nov. 1975.
[21] T. T. Wu and R. W. P. King, "The cylindrical antenna with nonreflecting resistive loading," *IEEE Trans. Antennas Propag.*, vol. AP-13, no. 3, pp. 369–373, May 1965.
[22] T. T. Wu and L. S. Shen, "Cylindrical antenna with tapered resistive loading," *Radio Sci.*, vol. 2, no. 2, pp. 191–201, 1967.

Marc Biancheri-Astier received the DESS degree (Professional Master degree) in electronic and telecommunication in 2005 and the DEA degree (Research Master degree) in signal processing in 2006 from the Université Sud-Toulon-Var, Toulon, France. He is currently working toward the Ph.D. degree in planetary subsurface exploration by ground-penetrating radar in the Laboratoire Atmosphère, Milieux, Observations Spatiales, Guyancourt, France. He works on characterization and optimization of the Electromagnetic Investigation of the SubSurface (EISS) performance.

He was a DEA Intern with the Laboratoire de Sondages Electromagnétiques de l'Environnement Terrestre (LSEET), CNRS, Toulon, where his field of interest turned to remote sensing with the development of UHF radar using the time reversal.

Valérie Ciarletti received the B.S. degree in engineering from the Ecole Centrale de Paris, Châtenay Malabry, France, in 1984, and the Ph.D. degree from the University of Paris 6, Paris, France, in 1989.

Since 2008, she has been a Professor with the Université de Versailles Saint-Quentin-en-Yvelines, Guyancourt, France. In 1993, her field of interest turned to microwave remote sensing (ground-penetrating radars and radars devoted to surface remote sensing). She is also currently with the Laboratoire Atmosphère, Milieux, Observations Spatiales. She was the Deputy Principal Investigator in the Netlander GPR project and is the Principal Investigator of the Water Ice and Subsurface Deposit Information On Mars (WISDOM) instrument selected on the ExoMars mission and Electromagnetic Investigation of the Sub Surface (EISS) instrument proposed for future space missions to Mars or others planets.

Alain Reineix received the Ph.D. degree in electronic and communications from the Institut de Recherche en Communications Optiques et Microondes (IRCOM) Laboratory, University of Limoges, Limoges, France, in 1986.

He was with the Centre National de la Recherche Scientifique (CNRS) first as a Researcher and then as a Professor. Since 2000, he has been the Head of the Electromagnetic Diffraction Team with the XLIM Institut de Recherche (formerly the IRCOM), Limoges. He was the first to introduce time domain methods (finite-difference time domain approach) in the radar cross-section computation of complex structures around their resonant frequencies and in the modeling of photoconductors for switching energy or generating short pulses.

Charlotte Corbel received the B.S. degree in engineering from the Ecole Nationale Supérieure des Télécommunications de Bretagne, Brest, France, and the M.S. degree in spacecraft technologies and satellite communications from the University College of London, London, U.K., in 2002.

Since 2003, she has been with Centre d'étude des Environnements Terrestre et Planétaires (currently, Laboratoire ATmosphère, Milieux, Observations Spatiales), Guyancourt, France, where she worked on radars and radiometer developments and, since 2005, she has been an Instrument Project Manager of the Water Ice and Subsurface Deposit Information On Mars and the Electromagnetic Investigation of the Subsurface Ground Penetrating Radars proposed on the ExoMars mission.